The Journal of the Oceanological Society of Korea
Vol. 21, No. 4, p. 203~210, December 1986.

A Simple Theoretical Model for the Upwind Flow in the Southern Yellow Sea

Young-Hyang Park

Department of Oceanography, Cheju National University, Cheju, Aradong, Korea

황해남부의 역풍류에 대한 단순 이론 모델

박 용 향

제주대학교 해양학과

Abstract

A linear parallel transport model is formulated and applied to an idealized Yellow Sea. With this simple analytical model, the hither-to suspected upwind flow phenomena in the southern Yellow Sea can be reasonably explained. In deep waters where the local depth exceeds a critical depth (H_c = 53m in the present model sea), pressure gradient force dominates over wind stress and contributes to an upwind flow. The estimated upwind flow velocity increases with wind speed and a maximum upwind flow occurs along the axis of the Yellow Sea embayment. For the typical south wind of 5-10 knots in summer, the upwind (southward) flow velocity along the axis of the Yellow Sea is estimated to be 1-5 cms^{-1}. While, for the typical north wind of 10-15 knots in winter, the upwind (northward) flow velocity is 5-12 cms^{-1}. These velocity ranges can be served as rough estimates for the intrusion velocity of the Yellow Sea Bottom Cold Water in summer and the Yellow Sea Warm Current in winter, respectively.

요약 : 선형, 평행 수송모델을 세우고 이상적인 황해에 적용하였다. 이 간단한 해석 모델로서 지금까지 예지되어 온 황해 남부의 역풍류 현상을 적절히 설명할 수 있다. 수심이 임계수심(본 모델 바다에서는 H_c=53m임)보다 깊은 해역에서는 압력 경도력이 바람응력보다 우세하여 역풍류를 야기시킨다. 추정된 역풍류 속도는 풍속과 함께 증가하며 최대 역풍류는 황해의 깊은 골을 따라 나타난다. 하계의 전형적인 남풍속도 5-10노트에 대해서 황해골을 따른 역풍류(남향류) 속도는 1-5cm s^{-1}로 추정된다. 반면에 동계의 전형적인 북풍속도 10-15노트에 대해서는 역풍류(북향류) 속도는 5-12cm s^{-1}이다. 이와 같은 속도 범위는 각각 하계의 황해 저층냉수와 동계의 황해 난류의 잠입속도에 대한 개략적인 추정치로서 사용될 수 있다.

INTRODUCTION

It has long been suspected from various hydrographic studies that there appear in the southern Yellow Sea a northward intrusion of the Yellow Sea Warm Current in winter and a southward extension of the Yellow Sea Bottom Cold Water in summer. These seasonally distinct phenomena might be recognized by a tongue-like distribution of warm (cold) waters pointing northward (southward) along the axis of the Yellow Sea in winter (summer) (Fig. 1). However, the typical wind system in the Yellow Sea can be characterized by stronger northerly winds in winter and weaker southerly winds in summer (Huh, 1982). Thus the northward flow of the Yellow Sea Warm Current and the southward flow of the Yellow Sea Bottom Cold Water, if they exist, represent the upwind (against the wind) flow in each

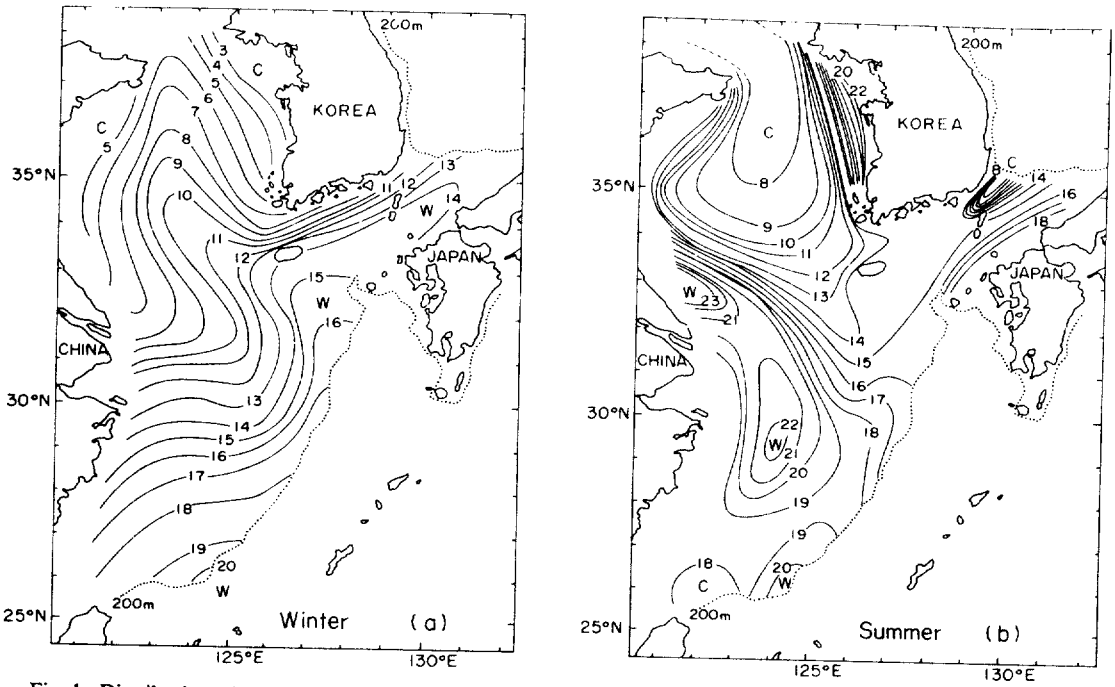

Fig. 1. Distribution of mean water temperatures (°C) at 50 m in the Yellow and East China Seas in winter (Jan.-Mar.) (a), and in summer (July-Sept.) (b) (After Kondo, 1985).

season. Some numerical model studies also show such upwind flows in deep waters along the axis of the Yellow Sea (Choi, 1982; Yuan and Su, 1983; Hsueh et al., 1985). Based on his numerical experiments on currents driven by a steady uniform wind stress in the Yellow and East China Seas, Choi (1982) pointed out that there appears strong downwind flows along the both sides of the Chinese coast and the west coast of Korea and the upwind flow in the middle of the Yellow Sea (Fig. 2).

Until now, we have no systematic current measurement data in the region. For some practical or scientific reasons, however, one may inquire how shall be the order of magnitude of such upwind flows and what are dynamical interpretations of the phenomena in question. Based on an analytical solution of frictionless, inertial model Csanady (1982) demonstrated that the dynamical effects of variable depth are responsible for the appearence of topographic gyres in shallow basins like Lake Ontario. The major objective of the present paper is to estimate the upwind flow velocity in the Yellow Sea on the basis of analytical model calculations of wind driven, frictionally controlled, parallel flow in a semi-enclosed basin of simple geometry.

In the following Chapter, a linear 'parallel transport model' with an idealized Yellow Sea topography is formulated. Estimate of the upwind velocity for different wind stresses is made in Chapter 3. Force balance within the upwind flow and downwind (following the wind) flow regions of the model sea is discussed in Chapter 4.

FORMULATION OF THE PARALLEL TRANSPORT MODEL

a) Fundamental equations

The model is based on the following depth-integrated or transport equations for a homogeneous shallow sea, using (x, y, z) coordinates with z-axis vertically up (Csanady,

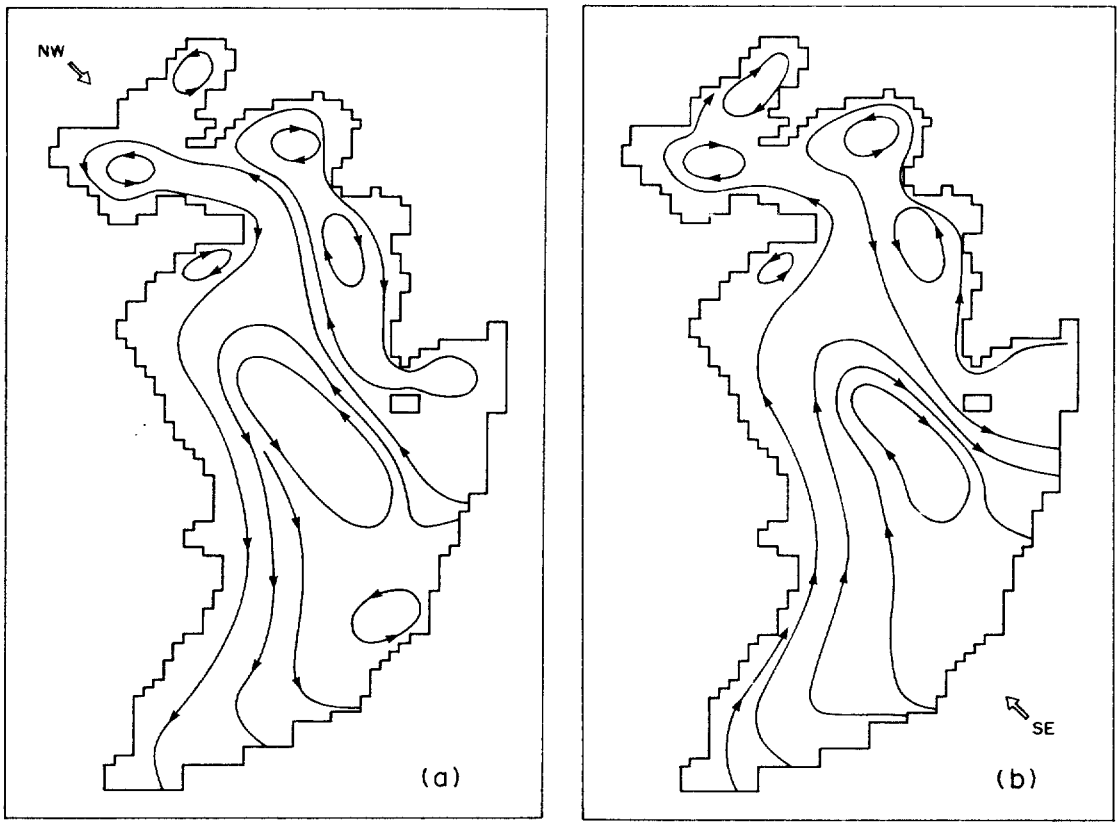

Fig. 2. Stream lines of wind driven currents produced by a uniform NW (a) and SE (b) wind stress of 10 dyn/cm² (After Choi, 1982).

1982):

$$\frac{\partial U}{\partial t} - fV = -gH\frac{\partial \eta}{\partial x} + F_x - B_x \quad (1)$$

$$\frac{\partial V}{\partial t} + fU = -gH\frac{\partial \eta}{\partial y} + F_y - B_y \quad (2)$$

$$\frac{\partial U}{\partial x} + \frac{\partial V}{\partial y} = -\frac{\partial \eta}{\partial t} \quad (3)$$

where U,V are horizontal transports defined by depth-intergration of the horizontal velocity components u,v, such as:

$$U = \int_{-H}^{0} u\,dz, \quad V = \int_{-H}^{0} v\,dz$$

where H is the depth of the bottom below mean sea level (z=0), g is gravity, η is the free surface elevation above mean sea level, f is the Coriolis parameter, and (F_x, F_y), (B_x, B_y) represent respectively wind stress and bottom stress components.

The analytical solution of Equations (1)-(3) in their general form is quite difficult, but made easier by making a number of idealizations in suitably simple models of coastal circulation.

b) Basic assumptions and parallel transport model

Consider a shallow embayment of simple geometry, closed at one end; Depth contours are straight and parallel to long straight coasts coincident with the y-axis, H = H(x) except in the end region where isobaths are closed (Fig. 3).

A uniform wind is supposed to act along the y-axis, $F_x = 0$, $F_y = F$, and the motion and

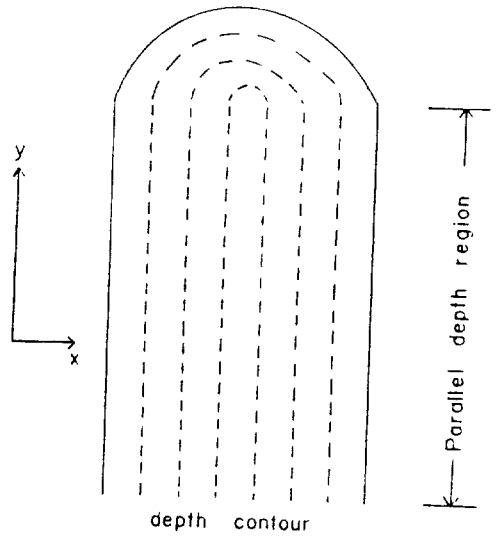

Fig. 3. Schematic of a semi-closed embayment with parallel depth region, in which depth contours are straight and parallel to long strait coasts.

the sea-level elevation are assumed to have reached a steady state. In this simple and idealized case, the longshore transport along an isobath in the parallel depth region may be expected to remain nearly constant, $\frac{\partial V}{\partial y} \simeq 0$. There is no reason why the steady state longshore transport within the parallel depth region varies significantly in the alongshore direction, especially under a uniform alongshore wind stress. However, in the vicinity of the head of embayment the coastal constraint may cause a significant variation of longshore transport along the y-axis. For mathematical simplicity, we restrict the discussion to the parallel depth region where the relation $\frac{\partial V}{\partial y} \simeq 0$ is expected to hold valid. In this case, the continuity equation (3) for steady-state flow ($\frac{\partial}{\partial t} \equiv 0$) implies $\frac{\partial U}{\partial x} \simeq 0$, so that U remains almost constant in a cross-section within the parallel depth region. In addition, it is reasonable to state that the transport in the vicinity of parallel coasts is dominantly in the alongshore direction and the cross-shore transport is negligible. This statement together with the relation, $\frac{\partial U}{\partial x} \simeq 0$ may suggest that the cross-shore transport within the entire parallel depth region is negligible, i.e., $U \simeq 0$, so that the net transport is dominantly along the isobaths, parallel to the straight coasts. This assumption ($U \simeq 0$) may be most critical and also criticizable in the present parallel transport model but there are experimental evidences which support qualitatively its validity; some hydrography and wind driven circulation models in a semienclosed shallow basin such as the Yellow Sea embayment (Kondo, 1985; Choi, 1982; Huseh et al., 1985) demonstrate the general flow pattern which follows approximately bottom topography.

In this study, the kinematic bottom stress is paramaterized by a following linear friction law:

$$B_x = \gamma \frac{U}{H}, \quad By = \gamma \frac{V}{H}$$

where γ is a resitance coefficient. Under the assumptions made previously for the flow within the parallel depth region (i.e.,

$$\frac{\partial}{\partial t} \equiv 0;\ F_x = 0;\ F_y = F;\ \frac{\partial V}{\partial y} = 0;$$

$$U = 0;\ B_x = \gamma \frac{U}{H};\ B_y = \gamma \frac{V}{H}),$$

Equations (1)-(3) reduce to:

$$-fV = -gH \frac{\partial \eta}{\partial x} \tag{4}$$

$$0 = -gH \frac{\partial \eta}{\partial y} + F - \gamma \frac{V}{H} \tag{5}$$

$$\frac{\partial V}{\partial y} = 0 \tag{6}$$

Equation (4) shows that the longshore transport V is in geostrophic equilibrium with the cross-shore sea-level gradient. Equation

(5) implies, dividing its right hand side by the Coliolis factor f, that the geostrophic cross-shore transport associated with the longshore sea-level gardient $(-\frac{gH}{f}\frac{\partial \eta}{\partial y})$ is balanced with the sum of Ekman transport in the suface layer $(\frac{F}{f})$ and Ekman transport in the bottom layer $(-\frac{By}{f})$. Thus, the parallel transport model of this kind shows completely different aspects of flow dynamics from those of pure drift currents by Ekman theory. In the present model, the sea-level elevation associated with the wind set-up and the effects of variable depth, which are not taken into account in the classic Ekman theory, could be most important dynamic factors.

The continuity equation (6) implies that the longshore transport is a function of distance from shore only, V = V(x), and the total transport at any cross-section has to vanish due to the coastal constraint and the steady-state surface elevation:

$$\int_{x_1}^{x_2} V dx = 0 \tag{7}$$

where x_1 and x_2 are the coordinates of the shores. A rearrangement of Equation (5) yields:

$$V = \frac{H}{\gamma} F - \frac{gH^2}{\gamma}\frac{\partial \eta}{\partial y} \tag{8}$$

Equation (4) shows that with H = H(x), $\frac{\partial V}{\partial y} = 0$, $\frac{\partial^2 \eta}{\partial x \partial y} = 0$ so that the longshore pressure gradient is independant of distance from shore, $\frac{\partial \eta}{\partial y} \equiv f(y)$. Substituing (8) into (7), and considering constant values of γ, F, it is possible to calculate the elevation gradient:

$$\frac{\partial \eta}{\partial y} = \frac{S_1}{gS_2} F \tag{9}$$

where S_1 is the cross-sectional area of the embayment

$$S_1 = \int_{x_1}^{x_2} H dx \tag{10}$$

and S_2 is defined by

$$S_2 = \int_{x_1}^{x_2} H^2 dx \tag{11}$$

within the parallel depth region. Substituing (9) into (8), the longshore transport may then be written as:

$$V = \frac{H}{\gamma} F \left(1 - \frac{HS_1}{S_2}\right) \tag{12}$$

This is the steady-state solution of the parellel transport model in which the cross-sectional transport is assumed to be zero, U = 0.

It can be easily seen from (12) that the longshore transport increases linearly with wind stress and its distribution in a cross-section is implicitely expressed in terms of the depth distribution, H(x). The transport vanishes where $H = S_2/S_1$ and the downwind flow is produced in shallower water, $H < S_2/S_1$, while the upwind flow appears in deeper water, $H > S_2/S_1$.

ESTIMATE OF UPWIND FLOW VELOCITY IN THE YELLOW SEA

The Yellow Sea posseses in general very complicated coast lines and depth distribution, characterized by a deepest water along the axis of the sea and a gradual reducing of a depth to zero at shores. However, the southern part of the Yellow Sea shows a relatively simple topography compared to the northern part of the sea. In order to get an idea of the order of magnitude for upwind flow velocity in the southern Yellow Sea, an idealized model sea as shown in the parallel transport model (Fig. 3) is considered. For a maximum simplicity, the depth distribution at a typical cross-section in the southern Yellow Sea is schematized by linear bottom slopes: -1/3750

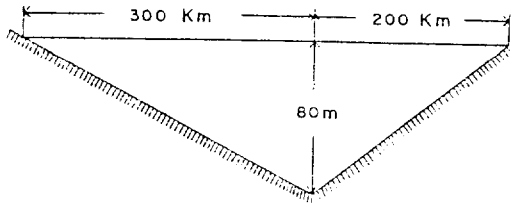

Fig. 4. Schematic of an idealized depth distribution at the typical cross-section in the southern Yellow Sea.

in the western part and 1/2500 in the eastern part (Fig. 4).

Making use of Equations (10) and (11) we obtain $S_1 = 20\ Km^2$ and $S_2 = 16/15\ Km^3$, so that the calculated transport is zero along the isobath of $H = S_2/S_1$ or $H \simeq 53$ m.

The transport distribution in the section can be obtained by specifying the longshore wind stress, F and the bottom resistance coefficient, γ. The magnitude of the kinematic wind stress F is specified by a quardratic drag law (Csandy, 1982):

$$F = \rho_a/\rho_w\ C_D W_{10}^2$$

where ρ_a/ρ_w is air-water density ratio which is nearly equal to 1.25×10^{-3}, W_{10} is wind speed measured at a height of 10 m, and C_D is the corresponding empirical drag coefficient given by

$$C_D = 1.6 \times 10^{-3},\quad W \leqq 7 ms^{-1}$$
$$C_D = 2.5 \times 10^{-3},\quad W \geqq 10 ms^{-1}$$

with a smooth transition for wind speed between 7 and 10 ms^{-1}. The specification of γ is rather arbitrary, however, we adapted here $\gamma = 0.05$ cm s^{-1} which seems to be the typical value of γ in the coastal ocean (Csanady, 1982).

Using the idealized depth distribution in the southern Yellow Sea (Fig. 4), the transport distribution for constant longshore wind of 5 ms^{-1} as an example is obtained (Fig. 5). As already indicated, the zero-transport appears along the isobath of H = 53 m and the upwind flow is confined within a deeper area (H>53 m). The maximum upwind transport appears

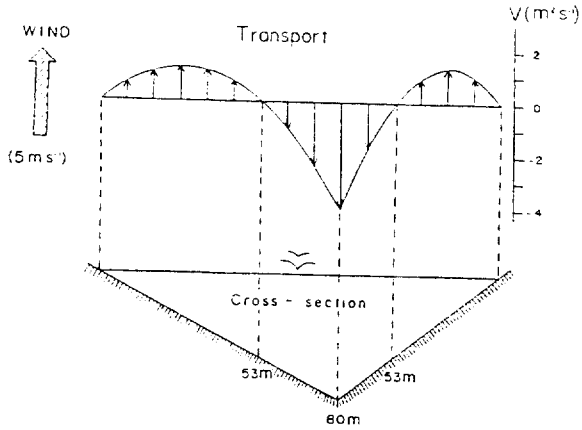

Fig. 5. Distribution of wind-driven transport in the idealized cross section of the southern Yellow Sea. The contant longshore wind of 5 ms^{-1} is applied.

in deepest water, H = 80 m.

The transport distribution in any section within the parallel depth region corresponds to the calculated pattern (Fig. 5), so that the transport streamlines shall be parallel each other but pointing in opposite directions at the center and at the shores. With the present simple model the transport distribution in the end region can not be obtained, however, it may be elucidated qualitatively: the streamlines there must close and the details may depend on the local topography. Fig. 6 illustrates a possible distribution of transport streamlines in the model sea, showing the upwind flow at the center and the downwind flow at the shores. This is analogous to topographic gyres which were discussed in Csanady (1982) for transient flow over variable depth. For the reversed wind the distribution pattern of stream lines remains unchanged but their senses are reversed.

Table 1 shows the calculated depth-mean velocity, V/H along the isobath of H = 80 m, for different wind speeds.

The depth-mean velocity in the upwind flow region is proportional to the local depth H (see Eq. 12), so that the calculated velocities in Table 1 coincide with the upper limit of the

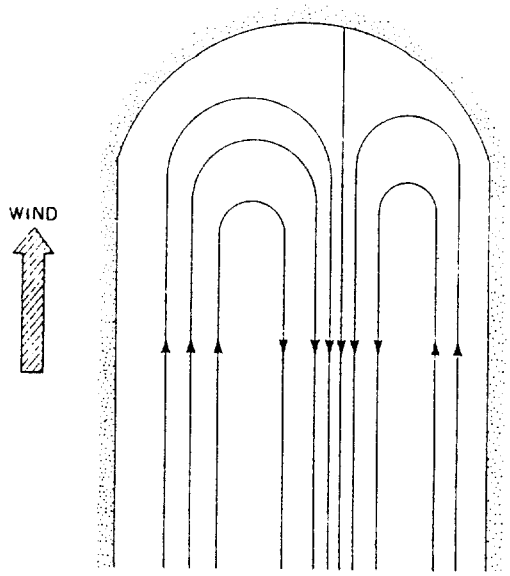

Fig. 6. Schematic of wind-driven transport streamlines in the model sea.

upwind flow velocity in our model sea, for different wind speeds or wind stresses. It is to be noted that the upwind flow velocity increases with wind speed. For the typical north wind of 10-15 knots in winter the maximum northward flow is 5-12 cm s^{-1}, which is of the same order of magnitude as that of Asaoka and Moriyasu (1966) who obtained, by a different method, 8 cm s^{-1} for NW wind of 7 m s^{-1} ($\simeq$14 knots). For the typical south wind of 5-10 knots in summer, the estimate of the maximum southward flow velocity in the southern Yellow Sea is 1-5 cm s^{-1}.

Table 1. Calculated depth-mean velocity, V/H along the axis of the model sea (H = 80 m), for different wind speeds or wind stresses. The estimate of the Ekman depth is made using an empirical formula; D(m) = 4.3 W(ms^{-1}) /$\sqrt{\sin\phi}$ (Bowden, 1983), with ϕ = 35 °N.

Wind Speed		Wind Stress	Depth Mean Velocity	Ekman Depth
W(ms^{-1})	(Knots)	F × 10^4 (m^2s^{-2})	V/H (cm s^{-1})	D(m)
2.5	(5)	0.125	1.3	14
5.0	(10)	0.500	5.0	28
7.5	(15)	1.230	12.3	43
10.0	(20)	3.125	31.3	57

DISCUSSION AND CONCLUSIONS

The estimate of the upwind flow velocity for different wind speeds in the southern Yellow Sea has been made. Here, we will examine briefly the underlying dynamics which are responsible for the appearence of the upwind flow in deep waters and the downwind flow in shallow coastal waters. The longshore momentum balance equation (5) indicates that the zero-transport occurs at some critical isobath, Hc where the longshore wind stress is exactly balanced by the depth-integrated longshore pressure gradient force: $F = gH\frac{\partial \eta}{\partial y}$. In shallow waters where $H < Hc$, especially near coasts, the wind stress dominates, $F > gH\frac{\partial \eta}{\partial y}$ and the transport is in the direction of the wind stress, so that the downwind flow occurs. In deeper waters where $H > Hc$, especially along the axis of the embayment, the pressure gradient force dominates, $F < gH\frac{\partial \eta}{\partial y}$ and the transport is in opposition to the wind stress, so that the upwind flow occurs. This simple explanation for the upwind flow is consistant with the results of numerical model runs for the 1980-1981 winter by Hsueh et al. (1985) who found that the pressure gradient force dominates in deep waters along the axis of the Yellow Sea embayment and contributes to an upwind (northward) flow.

In our Yellow Sea model, the critical isobath is determined only by the depth distribution, $Hc = S_2/S_1$. It is interesting to remark that the calculated critical isobath, Hc = 53 m coincides quite reasonably with the frontal isobath of the Yellow Sea Bottom Cold Water in summer in the southern Yellow Sea (Park, 1986). The present analytical model, though it is overidealized in some sense, may be used for making a simple estimate of the velocity of the Yellow Sea Bottom Cold Water in summer and of the Yellow

Sea Warm Current in winter, which are the hither-to suspected upwind flow phenomena in the southern Yellow Sea.

Equation (4) indicates that the depth mean velocity, V/H is in geostrophic balance with the cross-shore pressure gradient, $\frac{\partial \eta}{\partial x}$. The interior velocity at a depth, v(z) can be then considered as a sum of the Ekman layer velocity, v_E and the geostrophic velocity, $v_g = V/H$, i.e., $v(z) = v_E + v_g$. As the Ekman layer velocity decreases exponentially with increasing distance from the surface and becomes negligible outside the Ekman layer, the flow at depth is practically equal to the geostrophic velocity or the depth mean velocity. Considering the south wind of 5-10 knots in summer as an example, the Ekman depth for the wind of 5-10 knots is 14-28 m (see Table 1), which is relatively shallow compared to the local depths within the upwind flow region (H>53 m). Thus, the Yellow Sea Bottom Cold Water in summer which is generally located below 40 m (Park, 1986) and bounded by its frontal isobaths of about 50 m shall move southward. The upwind flow velocity increases with the local depth, so that the strongest upwind flow occurs along the axis of the Yellow Sea where the depth is maximum. For the typical south wind of 5-10 knots in summer, a maximum southward velocity of the Yellow Sea Bottom Cold Water is then estimated to be 1-5 cm s^{-1}. With a similar argument, a maximum northward velocity of the Yellow Sea Warm Current in winter can be estimated to be 5-12 cm s^{-1}, for the typical north wind of 10-15 knots.

ACKNOWLEDGMENTS

The work is carried out during my visit in the Department of Oceanography, Seoul National University during 1986. The author appreciates Drs. Kuh Kim and Im-Sang Oh for their reading the manuscript and useful comments. Financial support is given from a research fund of the Ministry of Education.

REFERENCES

Asaoka, O. and S. Moriyasu, 1966. On the circulation in the East China Sea and the Yellow Sea in winter. Oceanogr. Magazine, Vol. 18: 73-81.

Bowden, K.F., 1983. Physical oceanography of coastal waters. Ellis Harwood Ltd., 302 pp.

Choi, B.H., 1982. Note on currents driven by a steady uniform wind stress on the Yellow Sea and the East China Sea. La Mer 20: 30-38.

Csandy, G. T., 1982. Circulation in the coastal ocean. D. Reidel Pub. Co., 279 pp.

Hsueh, Y., R.D. Romea and P.W. Dewitt, 1985. Wintertime winds and coastal sea-level fluctuations in the northeast China Sea, Part II: Numerical Model. Submitted to the Journal of Physical Oceanography.

Huh, O.K., 1982. Satellite observations and the annual cycle of surface circulation in the Yellow Sea, East China Sea and Korea Strait. La Mer 20: 69-81.

Kondo, M., 1985. Oceanographic investigations of fishing grounds in the East China Sea and the Yellow Sea: Characteristics of the mean temperature and salinity distributions measured at 50 m and near the bottom. Bul. Seikai Regional Fish. Res. Lab., No. 62: 19-66.

Park, Y.H., 1986. Water characteristics and movements of the Yellow Sea Warm Current in summer. Submitted to the Deep-Sea Research.

Yuan, Y. and J. Su, 1983. A two-layer circulatrion model of the East China Sea. in Proceedings of International Symposium on Sedimentation on the Continental Shelf, with Special Reference to the East China Sea, Vol. 1, China Ocean Press, pp. 364-374.

Received July 8, 1986
Accepted October 30, 1986